communications earth & environment

Article

https://doi.org/10.1038/s43247-024-01247-4

Global ecosystem responses to flash droughts are modulated by background climate and vegetation conditions

Check for updates

Sungmin O[1] & Seon Ki Park[1,2,3] ✉

Flash droughts and their physical processes have received increasing attention in recent years due to concerns about the potential of flash droughts to affect water resources and ecosystems. Yet to date, the response of ecosystems during flash drought events, particularly on a large scale, and the determinants of the ecosystem responses to flash droughts have been underexplored. Here we analyse temporal variations in vegetation anomalies during flash drought events at a global scale between 2001 and 2020 using observation-based leaf area index, gross primary productivity, and solar-induced chlorophyll fluorescence data. We identify divergent ecosystem responses in terms of the timing and intensification of drought-induced vegetation stress across different regions around the world. Furthermore, we find that these regional differences are largely modulated by background climate and vegetation conditions, rather than meteorological conditions, with ecosystems being subjected to more rapidly developing and greater degrees of vegetation stress in arid and short vegetation-dominated regions as compared to humid forests. Our results highlight the spatially heterogeneous ecological impacts of flash droughts, implying the need to comprehensively integrate aspects of both atmospheric and bioclimatic properties in flash drought monitoring and forecasting systems to improve our ability to track their evolution and impacts.

Flash droughts are characterised by their unusually rapid intensification over sub-seasonal time scales and can occur anywhere in the world[1–4]. Flash droughts are primarily driven by a deficit in precipitation, but evolve rapidly in combination with other environmental anomalies, such as high temperatures, strong winds, or abundant radiation contributing to enhanced evaporative demand[3–7]. Flash droughts are therefore considered to be associated with compound extreme meteorological conditions, which can lead to ecological drought conditions that may have direct impacts on ecosystems[8,9]. There is thus a growing awareness of the need for fast responses to flash droughts. However, current monitoring and forecasting systems are mostly designed for slower-developing conventional droughts; thus, they may not serve as reliable early warning systems of flash droughts[2,10].

In order to comprehensively capture the complex evolution and impacts of flash droughts, previous studies have focused on a variety of drought-related meteorological, hydrological, and ecological anomalies as well as their temporal evolution throughout flash drought events. As the main drivers of flash droughts, precipitation and temperature generally exhibit consistent negative and positive anomalies, respectively, especially in the early stages of a flash drought[9,11,12]. Furthermore, their relative contributions to the initiation of a flash drought are the primary control on whether a given flash drought is driven by high temperatures or water deficiencies[11,13]. In contrast, vegetation-related variables such as evapotranspiration (ET) or gross primary production (GPP) often exhibit anomalies that rapidly change from positive to negative in the early stages a flash drought, especially in humid regions. For instance, vegetation health and functioning can be enhanced by the net radiation surplus associated with droughts when there is still available soil moisture during the onset of a flash drought[9,14,15]. As soil moisture continues to decrease, declining vegetation functioning can rapidly emerge within a few weeks. Therefore, detecting the direction of trends in vegetation anomalies (i.e. from increasing to decreasing trends) could be an effective indicator for monitoring worsening drought conditions and

[1]Department of Climate and Energy Systems Engineering, Ewha Womans University, Seoul, Republic of Korea. [2]Center for Climate/Environment Change Prediction Research, Ewha Womans University, Seoul, Republic of Korea. [3]Severe Storm Research Center, Ewha Womans University, Seoul, Republic of Korea. ✉e-mail: spark@ewha.ac.kr

impacts on ecosystems[16]. However, earlier studies have been limited to a few extreme events or to a country or several states. Consequently, the determinants of ecological responses to flash droughts remains underexplored, especially at large scales, such as across different climates or ecosystem regimes.

In addition, the magnitude and direction of vegetation anomalies provide direct indicators of the impact that flash droughts exert on ecosystems. Vegetation stress and mortality due to flash droughts have been quantified based on the analysis of temporal changes in various vegetation-related variables over many regions, including the US, Australia, India, or China[17–22]. Previous studies have suggested that the resistance of vegetation to droughts is not only associated with low water availability during drought events but is also closely related to regional characteristics, such as climate or vegetation type; these factors can significantly affect the degree to which flash droughts impact on ecosystems[9,23]. Nevertheless, a comprehensive global-scale assessment of regional differences in the ecological impact of flash droughts is still lacking.

Here we use observation-based leaf area index (LAI), gross primary production (GPP), and solar-induced chlorophyll fluorescence (SIF) data to investigate ecosystem responses during flash droughts at a global scale. To do this, we identify flash drought events between 2001 and 2020 at a 0.25° resolution based on soil moisture percentiles, and then examine the temporal variations in vegetation anomalies using composites across flash drought events that occurred in similar climate and vegetation regimes. Specifically, enabled by the large amount of employed global data, we focus on the spatial differences in the evolution of ecosystem structure and function over the course of flash droughts and the regional characteristics that can explain these spatial differences.

Results

Global flash drought occurrence across climate-vegetation regimes

Flash drought events are identified globally between 2001 and 2020 at a 0.25° × 0.25° spatial resolution, based on the rapid onset and intensification of soil moisture depletion (see Methods). Although there is no universal consensus on the definition or criteria of flash droughts[14,24], soil moisture is one of the most commonly used indicators[4,9,25] and its relevance to ecosystems is well known[26,27]. Given our research focus on the ecosystems, only growing seasons are considered in the analysis; this includes all months in the latitude range between 30°S and 30°N, March through October for the Northern Hemisphere, and September through April for the Southern Hemisphere.

The spatial distribution of flash drought occurrence in Fig. 1a shows that flash droughts can occur across all bioclimatic regimes, which are defined by long-term dryness index and tree-cover dominance (Fig. 1b). A higher likelihood of flash droughts is detected in the tropics and subtropics including northern South America, part of Africa including the Sahel, India, and Southeast Asia. Over most of these regions, more than about 10 flash drought events are identified during the study period (2001-2020), implying a frequency of more than one flash drought event every two years. While precipitation deficits turn out to be the dominant driver of flash droughts, most flash droughts occurred under simultaneous drier and warmer conditions; approximately 87% of total flash droughts occurred under drier conditions, and around 70% of them occurred under warmer conditions (Fig. S1 in Supplementary). The spatial patterns of flash drought frequency presented here are broadly consistent with global flash drought hotspots reported in previous studies[3,6,28]. However, some local-scale differences exist,

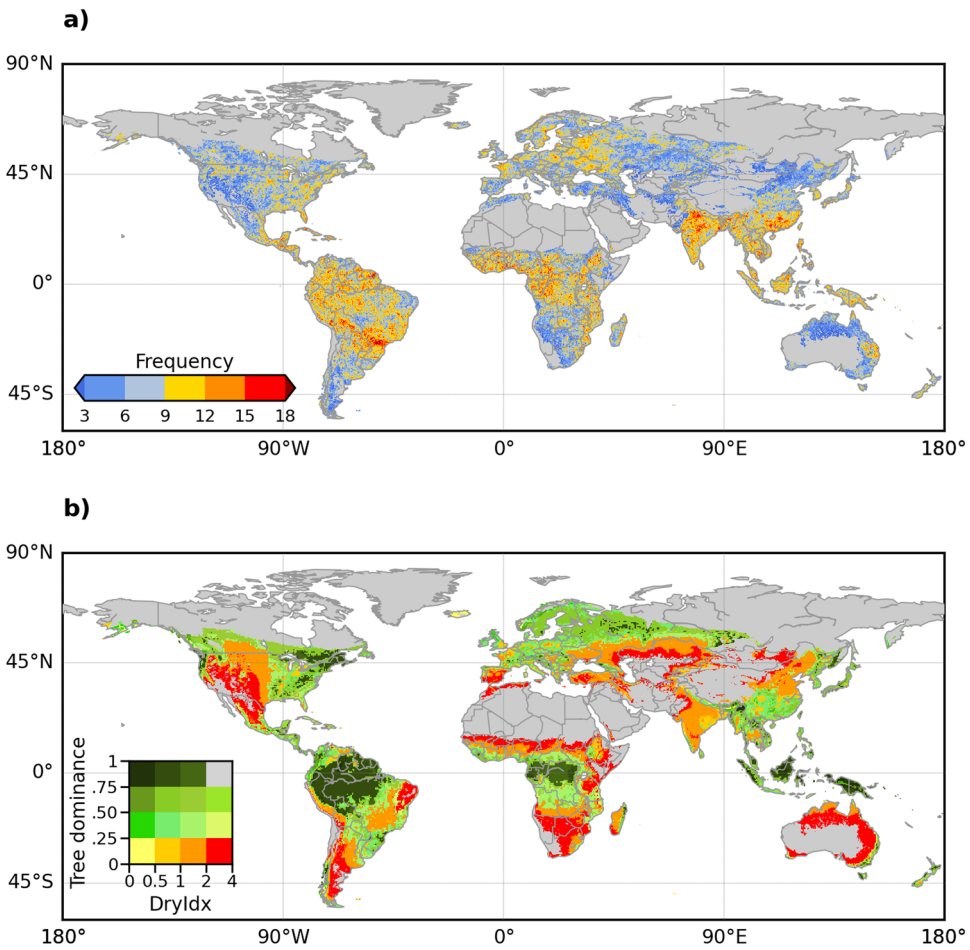

Fig. 1 | Flash drought occurrence and climate-vegetation regimes. a Flash drought frequency computed from ERA5 reanalysis soil moisture data (30 cm depth) over growing seasons between 2001 and 2020. **b** Climate-vegetation regimes defined by long-term dryness index and tree-cover dominance. Too arid or cold grid pixels are excluded. See Methods for more details. See also Fig. S2 for complementary analysis with SoMo.ml observation-based data[30] and ERA5 deeper layer soil moisture data (60 cm depth). The map is created using the Matplotlib basemap v1.2.2 toolkit[57].

such as in Australia[3,13,29] or Europe[3,25], which are likely to have arisen due to the use of inconsistent frameworks for identifying flash drought events among the studies, including different indicators, datasets, and spatial resolutions or study periods. Using both observation-based soil moisture data[30] and deeper layer soil moisture data (60 cm depth), we confirm that although the absolute number of flash drought frequency per grid pixel can be altered, the overall spatial pattern remains the same regardless of soil moisture data or depth (Fig. S2).

Ecosystem responses to flash droughts

We select eight different geographical regions across the globe to investigate ecosystem responses during flash droughts, namely: Eastern North America (ENA), Central Europe (CEU), South Asia (SAS), East Asia (EAS), Northwestern South America (NWS), Southeastern South America (SES), West Africa (WAF), and Eastern Australia (EAU). While we select the regions with relatively high frequencies of flash drought events from Fig. 1a (e.g. SAS, EAS, and SES), which are also recognised as flash drought hotspots in previous studies[3,28], we also include diverse climate-vegetation regimes for consideration. As a result, four humid or subhumid (long-term dryness index < 1) and four arid or semiarid regions (dryness index > 1) with different ecosystem compositions are chosen. We then examine the temporal evolution of normalised anomalies (z-score) in soil moisture and LAI averaged across flash drought events within each region (Fig. 2). To account for data uncertainties, and to compare the (dis)similarities in spatiotemporal variations in vegetation structure and functioning, we also employ observation-based GPP and SIF data and report the corresponding results in Figs. S3 and S4.

Soil moisture declines rapidly within five pentads (25 days) during the onset of flash droughts, showing overall similar temporal patterns across all regions, as expected from the flash drought definition used in this study. However, relatively large differences among the regions are observed in terms of the peaks and recovery of soil moisture. Minimum soil moisture anomalies range from -1.57 to -1.06 on average, while recovery rates (rate of increase in soil moisture over a month after the drought peak) range from 0.07 to 0.23 per pentad.

There are greater regional differences in the temporal variations of LAI (greenness) compared to soil moisture. Furthermore, LAI anomalies are not always correlated with soil moisture anomalies, particularly in humid or subhumid regions. For instance, regions with a dryness index lower than 1, including ENA, CEU, EAS, and NWS, show increasing LAI anomalies in the early stages of flash droughts, which may contributed to more rapid depletion in soil moisture. Enhanced ecosystem indices, such as increased

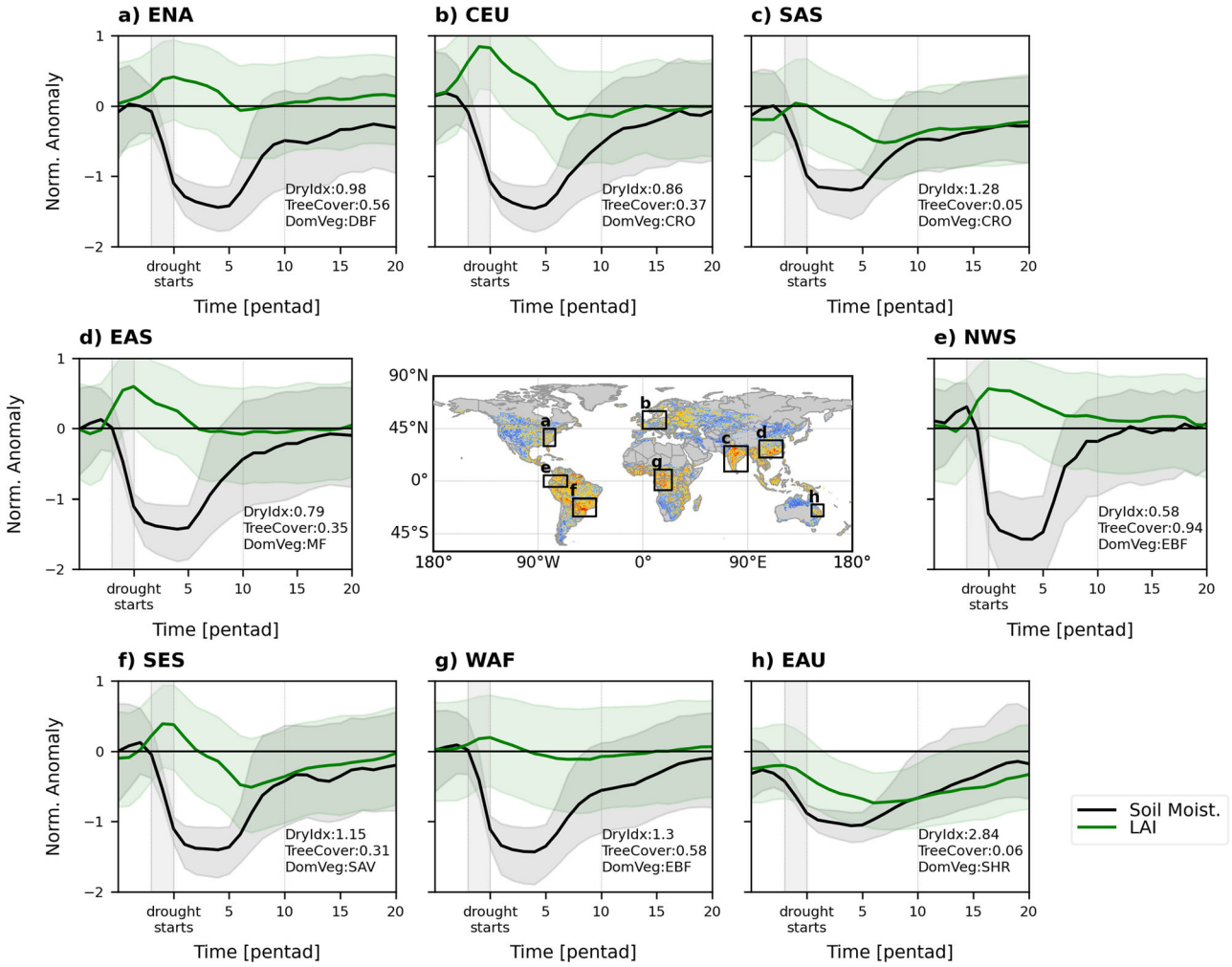

Fig. 2 | Divergent ecosystem responses to flash droughts. a–h Temporal variations in soil moisture (black line) and LAI (green) during flash drought events for the eight selected regions outlined in black on the map. Bold lines represent medians, while shaded areas represent variability (between the 25th and the 75th percentiles) observed across flash drought events. Vertical shaded areas indicate the onset stage of flash droughts. Regional dryness index and tree dominance are computed using the medians of all grid pixels within each region, and dominant vegetation type is based on the highest percentage of vegetation type across all grid pixels within each region. CRO represents croplands; DBF, deciduous broadleaf forests; EBF, evergreen broadleaf forests; MF, mixed forests; SAV, savannas; SHR, shrublands. GPP and SIF show similar temporal patterns with LAI (Figs. S3 and S4, respectively).

LAI or evapotranspiration during the drought development period, are frequently observed in humid, and thereby energy-limited climate regimes[9,31,32]. This is associated with drought-related clear sky conditions that favor more incoming solar radiation, which leads to vegetation greening[33]. Additionally, most of the selected humid regions consist of forested areas, such as temperate deciduous forest biome in ENA, mixed forests in EAS, or Amazonian evergreen forests in NWS. Trees are capable of avoiding drought stress through various strategies, such as limiting water loss through stomatal closure or shifting water uptake depths from surface to deep soil moisture[34,35]. As a result, in the humid regions, negative LAI anomalies are rarely detected over the course of flash droughts, even though spatial variability exists across individual grid pixels.

In contrast, negative LAI responses are more dominant in arid or semiarid regions, such as SAS, SES, WAF, and EAU, where the dryness index is higher than 1. In SES, where the dryness index is lower (i.e. relatively wetter) than the other arid regions, LAI is higher than usual for a period at the onset of flash drought, but it drops continuously as the drought progresses, and eventually becoming negative. In particular, SAS and EAU with a low tree dominance (0.05 and 0.06, respectively) show negative LAI anomalies already from the very early stages (onset and initiation phases) of flash droughts; arid ecosystems tend to rapidly respond to droughts[36], and plant growth in arid, water-limited climate regimes, is more sensitive to soil moisture availability[37]. In sum, it can be seen that the negative peak anomalies are larger and longer-lasting in SAS and EAU compared to the other regions. Meanwhile, the negative anomalies in LAI are much smaller in WAF, which is possibly related to its distinct ecosystems (mainly evergreen forests) with more effective strategies to cope with drought stress than short vegetation. Note that while WAF is conventionally considered a humid region, the dryness index over the study period is higher than 1, possibly reflecting the recent drying trends in the region[38].

While cropland is the dominant vegetation type both in CEU and SAS (52% and 74% of the area, respectively), the two regions show remarkably contrasting LAI responses. In CEU, positive or near-zero anomalies are observed over the course of flash droughts, whereas mostly negative anomalies are observed in SAS. This may be due to the different background climate regimes (i.e. subhumid and semiarid, respectively), and associated drought characteristics; for instance, droughts tend to last longer in arid regimes due to high soil moisture memory, with soil moisture anomalies in SAS actually remaining negative for a longer period. Furthermore, the possible dominance of differing crop types (e.g. wheat vs rice) between the regions may also explain the contrasting LAI patterns, as each crop type has its own level of water stress tolerance[39]. However, it should be noted that crop type is not assessed in this study, and should therefore be further investigated.

The diverse responses of regional ecosystems to flash droughts are also well captured in GPP and SIF (Figs. S3 and S4). A higher LAI generally indicates potential for higher photosynthetic capacity; thus, GPP expectedly shows overall similar patterns with LAI. However, GPP and SIF show a closer agreement with each other than either measure does with LAI, respectively. This is to be expected given that SIF is emitted by plants during photosynthesis, and has therefore been proposed as a good proxy of GPP[40]. Furthermore, we find relatively larger differences between LAI and GPP/SIF in NWS, which consists mainly of evergreen trees. The decoupling of LAI-GPP is often reported in previous studies[41], especially for forest ecosystems, where the trade-off between ecosystem structure (LAI) and physiology (photosynthesis per unit leaf) is stronger; dense canopy, for instance, can limit solar radiation and consequently reduce photosynthesis.

To assess the significance of the observed LAI anomalies, we randomly select the same n-th pentad in which the flash drought event occurred from a different year, and then re-compute Fig. 2. The averaged temporal evolution of LAI anomalies across flash drought events remains close to zero (Fig. S5), implying that the distinct LAI anomaly patterns found in the main analysis are caused by flash drought events.

Role of climate and vegetation in modulating flash drought impacts

We conduct further investigations into ecosystem responses during flash droughts at all grid pixels that occurred across different climate-vegetation regimes by defining the time taken for normalised LAI anomalies to shift from positive to negative values (referred to as 'Timing') and the magnitude of the maximum negative anomaly observed (referred to as 'Intensity'). These two metrics are computed for each bioclimatic regime, which is defined based on the long-term dryness index and tree-cover dominance (see Methods). We also repeat the analysis using GPP and SIF (see Figs. S6 and S7, respectively). More information about the regimes, including the proportion of area and dominant vegetation type, can be found in Fig. S8. Interestingly, both the timing and intensity exhibit remarkable spatial gradient patterns as the bioclimatic regimes shift from humid to arid regions, as well as from tree-dominated to short-vegetation regions (Fig. 3). As a result, more rapidly developing and larger negative LAI anomalies are observed in arid and short-vegetation dominated regions compared to humid forests.

In humid regions (dryness index < 1), where absolute soil moisture is still available even after the onset of the flash droughts, trees with deeper roots are assumed to reach the water table[34]; thus, the ecosystem can sustain its structure and water use for photosynthesis[34]. Humid forests are also energy-limited and may benefit from the ample energy available during the early stages of droughts[31,32], as seen in the cases of ENA, EAS, or NWS in Fig. 2. Moreover, water-saving strategies of trees (e.g. stomatal closure) are known to enable them to avoid and tolerate drought stress[34,42], resulting in overall smaller negative peaks of LAI. On average, humid regions with forests (tree dominance > 0.5), and with a great presence of evergreen and mixed forests (Fig. S8), do not show any negative LAI responses. It should be noted, however, that since we examine the composites of the averaged temporal evolutions of LAI across many grid pixels, negative anomalies can nonetheless be observed in some of the individual grid pixels.

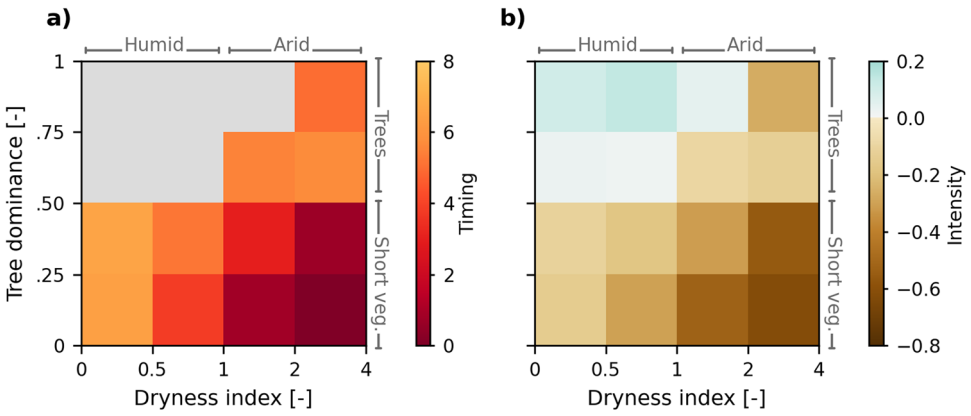

Fig. 3 | Timing and intensity of flash drought impact on ecosystems. a the average pentads taken for the LAI anomaly to become negative after the onset of a flash drought (timing) and **b** the minimum value of the LAI anomaly (intensity) across climate-vegetation regimes. The timing and intensity values are computed using the median of the LAI time series across flash drought events within the same bioclimatic regime. Note that the timing in humid tree-dominated regimes marked with grey is not defined because the LAI anomaly does not show negative values during the entire duration of the flash drought. We find similar results with GPP and SIF (Figs. S6 and S7, respectively).

In contrast, in arid regions where soil moisture content plays an essential role in maintaining vegetation, negative LAI anomalies develop more rapidly and become more intense as flash drought progresses. This is particularly noticeable in less tree-dominated regions where grassland, savannah, or cropland prevails (Fig. S8), which could be attributed to the faster responses of short vegetation to drought conditions on short timescales and their tendency to lack water conservation mechanisms[36,42], as we speculate based on the cases of SAS and EAU in Fig. 2.

Given the dominant role of soil moisture in determining drought stress on ecosystems[26,43], flash drought characteristics, such as drought duration or intensity, can also be an important factor affecting ecosystem responses to flash droughts. While the spatial patterns of flash drought duration and intensity across the climate-vegetation regimes are not very clear, soil moisture dry-downs tend to last longer and be more severe in arid regimes (Fig. S9). Therefore, a higher chance of reaching below the critical soil moisture levels, the point at which plants start to experience water stress[43], can also explain the greater negative anomalies of LAI or GPP in the arid regimes.

Discussion

In a warmer future, more frequent and faster flash drought events are to be expected[44–47]. Flash droughts may have an irreversible impact on ecosystems as they do not have enough time to adapt to the sudden depletion in water availability and associated extreme conditions[9,23]. However, the timely monitoring and/or forecasting of flash droughts remains challenging, since current systems primarily target slowly-evolving drought events over longer time scales[2,10]. In addition to recent efforts to apply multivariate approaches to drought detection and monitoring, the closer investigation of vegetation responses beyond meteorological and hydrological anomalies during flash droughts can guide effective monitoring approaches and the development of early warning systems.

Recent progress in the ecological aspects of flash droughts has been made through case studies and regional analyses. These studies mostly focus on the overall impacts of flash droughts on ecosystems[18–22]. Here we use global-scale observational vegetation data and focus on regional differences in the temporal evolution of ecosystem responses to flash droughts. We show that the temporal dynamics of ecological anomalies are dominantly influenced by region-specific background climate or vegetation. While meteorological conditions are critical drivers of flash drought occurrences[11,12], our analysis does not find any clear spatial patterns regarding the contribution of precipitation or temperature anomalies during the onset stage of flash drought to the timing or degree of the ecological impacts of flash droughts (Fig. S10).

Specifically, our results highlight characteristic vegetation responses to water deficit during flash droughts that differ between regions, and consequently, spatially heterogeneous timing and degree of vegetation stress. Therefore, the integration of vegetation-related information and their interactions with climate and soil is critical for the reliable monitoring and prediction of vegetation dynamics under water stress. It is well-known that Earth system models often misrepresent soil-vegetation-atmosphere interactions and produce vegetation anomaly signals (e.g. evapotranspiration) that contradict observational data, especially during drought conditions[48,49]. On the other hand, the key findings in this study are based on ecosystem data of satellite observations or upscaled in-situ measurements. Therefore, our observation-based investigations into the temporal patterns of ecosystem responses and their regional differences can provide an advanced reference against which the performance of physics models on subseasonal scale drought predictions can be evaluated.

Here we define flash drought based on soil moisture percentiles. The definition of flash droughts has been the subject of debate, and there have been several proposed indices and thresholds that have been used to define their rapid onset and intensification[14]. We test different criteria by changing soil moisture percentile thresholds to define flash droughts and confirm that the overall results of this study are not sensitive to the chosen flash drought definition (Fig. S11). In addition, 8-day data are used for ecological variables in this study, and therefore daily extremes could be underestimated. Although this would not significantly affect our main findings, upcoming novel data with high spatio-temporal resolution satellite data (e.g. Sentinel-2 satellites) could provide more detailed information about vegetation responses during rapidly developing flash drought events.

The findings from this study can advance our understanding of the diverse ecosystem responses to flash droughts and provide insights into flash drought impact monitoring and early warning systems. Future works can include more detailed vegetation-related information considering diverse plant functional groups or rooting depth to provide a more comprehensive understanding of ecosystem dynamics during flash droughts. The propagation of flash to long-term droughts can also be considered, as recent studies show that flash droughts often develop into conventional droughts[50], and this transition to long-term droughts can significantly aggravate drought stresses.

Methods

Flash drought identification

We define flash droughts based on the rapid changes in soil moisture[9,13,25]. ERA5 reanalysis soil moisture data[51] in the top 30 cm depth, computed as a depth-weighted mean of the values in the first to third layers (0–7 cm, 7–28 cm, and 28–100 cm depths, respectively) are used. In each grid pixel, the soil moisture data are aggregated into 5-day averages, which are then converted into percentiles through the Gringorten plotting position approach[52]. A flash drought begins when the pentad-averaged soil moisture percentile declines from at or above the 40th percentile to below the 20th percentile within no more than five pentads. During the onset of drought, soil moisture percentiles should consistently decrease with a mean rate of at least 0.1 per pentad. The flash drought is considered to be terminated when the soil moisture increases back to above the 20th percentile and remains at that level for at least two consecutive pentads. A flash drought event is defined as having a duration of 6 to 18 pentads to exclude an insignificant short-term event and to distinguish it from a conventional, long-term drought[13,25]. We further use observation-based SoMo.ml data for complementary analysis reported in Fig. S2. SoMo.ml is generated using a machine learning algorithm that is trained to learn the relationships between multiple meteorological predictor variables and target in-situ soil moisture data[30].

Climate and vegetation regimes

To characterise the regional background climate, long-term dryness index, defined as the ratio of the long-term averaged equivalent evaporation (computed from net radiation by multiplying the inverse of the latent heat of vaporisation) to precipitation[31,49] over the entire 20-year study period, is calculated for each grid pixel (see Fig. S12). Both net radiation and precipitation data are obtained from the ERA5 reanalysis data. Tree-cover dominance is defined as the ratio of fractional tree cover to the total vegetation cover (tree and short vegetation) using the AVHRR satellite data from 2001 to 2016[53]. Dominant vegetation information is obtained from the GLDAS Land Cover Dataset based on MODIS vegetation data that uses a modified IGBP classification scheme.

Ecosystem variables

The main result of this study is based on LAI data obtained from gap-filled MODIS satellite data[54], while GPP data from FLUXCOM[55] and SIF data from GOSIF[56] are additionally used for supplementary analysis. FLUXCOM upscales point-level GPP measurements obtained from eddy covariances across the globe through data-driven approaches; machine learning models are trained on in-situ eddy covariance data to capture GPP variability using multiple predictor variables, and then they are used to estimate GPP globally. The native spatial resolution of the GPP is 0.5°, and thus we simply repeated the data both latitudinally and longitudinally to match the target spatial resolution. GOSIF is derived from a machine learning model trained with OCO-2 SIF data. All data are available at an 8-day scale, so we linearly interpolate the data into a daily scale and then aggregate to a pentad scale.

Data availability

ERA5 reanalysis data are available at https://cds.climate.copernicus.eu. MODIS LAI, FLUXCOM GPP, and GOSIF SIF data can be obtained from https://www.earthdata.nasa.gov, https://www.fluxcom.org, and https://globalecology.unh.edu, respectively. AVHRR Vegetation Continuous Fields data are available at https://lpdaac.usgs.gov/products/vcf5kyrv001/. GLDAS Land Cover Dataset is available at https://ldas.gsfc.nasa.gov/gldas/. The data for the main manuscript figures are available at https://github.com/osungmin/paper_NCEE2024_FlashDrought.git.

Code availability

The code used for this study is available at https://github.com/osungmin/paper_NCEE2024_FlashDrought.git.

Received: 31 July 2023; Accepted: 30 January 2024;
Published online: 19 February 2024

References

1. Koster, R. D., Schubert, S. D., Wang, H., Mahanama, S. P. & DeAngelis, A. M. Flash drought as captured by reanalysis data: Disentangling the contributions of precipitation deficit and excess evapotranspiration. *J. Hydrometeorol.* **20**, 1241–1258 (2019).
2. Pendergrass, A. G. et al. Flash droughts present a new challenge for subseasonal-to-seasonal prediction. *Nat. Clim. Chang.* **10**, 191–199 (2020).
3. Christian, J. I. et al. Global distribution, trends, and drivers of flash drought occurrence. *Nat. Commun.* **12**, 6330 (2021).
4. Yuan, X. et al. A global transition to flash droughts under climate change. *Science* **380**, 187–191 (2023).
5. Ford, T. W. & Labosier, C. F. Meteorological conditions associated with the onset of flash drought in the eastern United States. *Agric. For. Meteorol.* **247**, 414–423 (2017).
6. Deng, S., Tan, X., Liu, B., Yang, F. & Yan, T. A reversal in global occurrences of flash drought around 2000 identified by rapid changes in the standardized evaporative stress ratio. *Sci. Total Environ.* **848**, 157427 (2022).
7. Wang, Y. & Yuan, X. Land-atmosphere coupling speeds up flash drought onset. *Sci. Total Environ.* **851**, 158109 (2022).
8. Mahto, S. S. & Mishra, V. Increasing risk of simultaneous occurrence of flash drought in major global croplands. *Environ. Res. Lett.* **18**, 044044 (2023).
9. O, S. & Park, S. K. Flash drought drives rapid vegetation stress in arid regions in Europe. *Environ. Res. Lett.* **18**, 014028 (2023).
10. Otkin, J. A. et al. Getting ahead of flash drought: from early warning to early action. *Bull. Am. Meterol. Soc.* **10**, E2188–E2202 (2022).
11. Mo, K. C. & Lettenmaier, D. P. Precipitation deficit flash droughts over the United States. *J. Hydrometeorol.* **17**, 1169–1184 (2016).
12. Shah, J. et al. On the role of antecedent meteorological conditions on flash drought initialization in Europe. *Environ. Res. Lett.* **18**, 064039 (2023).
13. Qing, Y., Wang, S., Ancell, B. C. & Yang, Z.-L. Accelerating flash droughts induced by the joint influence of soil moisture depletion and atmospheric aridity. *Nat. Commun.* **13**, 1139 (2022).
14. Otkin, J. A. et al. Flash droughts: a review and assessment of the challenges imposed by rapid-onset droughts in the United States. *Bull. Am. Meterol. Soc.* **99**, 911–919 (2018).
15. Jiang, Y., Yang, M., Liu, W., Mohammadi, K. & Wang, G. Eco-hydrological responses to recent droughts in tropical South America. *Environ. Res. Lett.* **17**, 024037 (2022).
16. Mohammadi, K., Jiang, Y. & Wang, G. Flash drought early warning based on the trajectory of solar-induced chlorophyll fluorescence. *Proc. Natl Acad. Sci. USA* **119**, e2202767119 (2022).
17. Otkin, J. A. et al. Assessing the evolution of soil moisture and vegetation conditions during the 2012 United States flash drought. *Agric. For. Meteorol.* **218-219**, 230–242 (2016).
18. Jin, C. et al. The 2012 flash drought threatened US midwest agroecosystems. *Chin. Geogr. Sci.* **29**, 768–783 (2019).
19. Christian, J. I., Basara, J. B., Hunt, E. D., Otkin, J. A. & Xiao, X. Flash drought development and cascading impacts associated with the 2010 russian heatwave. *Environ. Res. Lett.* **15**, 094078 (2020).
20. Zhang, M., Yuan, X. & Otkin, J. A. Remote sensing of the impact of flash drought events on terrestrial carbon dynamics over China. *Carbon Balance Manag.* **15**, 20 (2020).
21. Poonia, V., Kumar Goyal, M., Jha, S. & Dubey, S. Terrestrial ecosystem response to flash droughts over India. *J. Hydrol.* **605**, 127402 (2022).
22. Yao, T., Liu, S., Hu, S. & Mo, X. Response of vegetation ecosystems to flash drought with solar-induced chlorophyll fluorescence over the Hai River Basin, China during 2001-2019. *J. Environ. Manage.* **313**, 114947 (2022).
23. Zhang, M. & Yuan, X. Rapid reduction in ecosystem productivity caused by flash droughts based on decade-long FLUXNET observations. *Hydrol. Earth Syst. Sci.* **24**, 5579–5593 (2020).
24. NOAA/National Integrated Drought Information System, Lisonbee, J., Woloszyn, M. & Skumanich, M. Making sense of flash drought: definitions, indicators, and where we go from here. *JoASC* **2021**, 1–19 (2021).
25. Shah, J. et al. Increasing footprint of climate warming on flash droughts occurrence in Europe. *Environ. Res. Lett.* **17**, 064017 (2022).
26. Liu, L. et al. Soil moisture dominates dryness stress on ecosystem production globally. *Nat. Commun.* **11**, 4892 (2020).
27. Liu, X., Feng, X. & Fu, B. Changes in global terrestrial ecosystem water use efficiency are closely related to soil moisture. *Sci. Total Environ.* **698**, 134165 (2020).
28. Mukherjee, S. & Mishra, A. K. A multivariate flash drought indicator for identifying global hotspots and associated climate controls. *Geophys. Res. Lett.* **49**, e2021GL096804 (2022).
29. Parker, T., Gallant, A., Hobbins, M. & Hoffmann, D. Flash drought in Australia and its relationship to evaporative demand. *Environ. Res. Lett.* **16**, 064033 (2021).
30. O, S. & Orth, R. Global soil moisture data derived through machine learning trained with in-situ measurements. *Sci. Data* **8**, 170 (2021).
31. Orth, R. & Destouni, G. Drought reduces blue-water fluxes more strongly than green-water fluxes in Europe. *Nat. Commun.* **9**, 3602 (2018).
32. O, S. et al. The role of climate and vegetation in regulating drought-heat extremes. *J. Clim.* **35**, 5677–5685 (2022).
33. Li, W. et al. Widespread and complex drought effects on vegetation physiology inferred from space. *Nat. Commun.* **14**, 4640 (2023).
34. Brunner, I., Herzog, C., Dawes, M. A., Arend, M. & Sperisen, C. How tree roots respond to drought. *Front. Plant Sci.* **6**, 547 (2015).
35. Kühnhammer, K. et al. Deep roots mitigate drought impacts on tropical trees despite limited quantitative contribution to transpiration. *Sci. Total Environ.* **893**, 164763 (2023).
36. Vicente-Serrano, S. M. et al. Response of vegetation to drought time-scales across global land biomes. *Proc. Natl Acad. Sci. USA* **110**, 52–57 (2013).
37. Knapp, A. K. et al. Field experiments have enhanced our understanding of drought impacts on terrestrial ecosystems-but where do we go from here? *Funct. Ecol*. 1365–2435.14460 (2023).
38. Greve, P. et al. Global assessment of trends in wetting and drying over land. *Nat. Geosci* **7**, 716–721 (2014).
39. Vijayaraghavareddy, P. et al. Acquired traits contribute more to drought tolerance in wheat than in rice. *Plant Phenomics* **2020**, 2020/5905371 (2020).
40. Pickering, M., Cescatti, A. & Duveiller, G. Sun-induced fluorescence as a proxy for primary productivity across vegetation types and climates. *Biogeosciences* **19**, 4833–4864 (2022).
41. Hu, Z. et al. Decoupling of greenness and gross primary productivity as aridity decreases. *Remote Sens. Environ.* **279**, 113120 (2022).

42. Teuling, A. J. et al. Contrasting response of European forest and grassland energy exchange to heatwaves. *Nat. Geosci.* **3**, 722–727 (2010).
43. Fu, Z. et al. Critical soil moisture thresholds of plant water stress in terrestrial ecosystems. *Sci. Adv.* **8**, eabq7827 (2022).
44. Hoffmann, D., Gallant, A. J. E. & Hobbins, M. Flash drought in CMIP5 models. *J. Hydrometeorol.* **22**, 1439–1454 (2021).
45. Mishra, V., Aadhar, S. & Mahto, S. S. Anthropogenic warming and intraseasonal summer monsoon variability amplify the risk of future flash droughts in india. *npj Clim. Atmos. Sci.* **4**, 1 (2021).
46. Sreeparvathy, V. & Srinivas, V. V. Meteorological flash droughts risk projections based on CMIP6 climate change scenarios. *npj Clim. Atmos. Sci.* **5**, 77 (2022).
47. Christian, J. I. et al. Global projections of flash drought show increased risk in a warming climate. *Commun. Earth Environ.* **4**, 165 (2023).
48. Zhao, M., A, G., Liu, Y. & Konings, A. G. Evapotranspiration frequently increases during droughts. *Nat. Clim. Chang.* **12**, 1024–1030 (2022).
49. Li, W. et al. Contrasting drought propagation into the terrestrial water cycle between dry and wet regions. *Earth's Future* **11**, e2022EF003441 (2023).
50. Wang, L. & Yuan, X. Two types of flash drought and their connections with seasonal drought. *Adv. Atmos. Sci.* **35**, 1478–1490 (2018).
51. Hersbach, H. et al. The ERA5 global reanalysis. *Q.J.R. Meteorol. Soc.* **146**, 1999–2049 (2020).
52. Gringorten, I. I. A plotting rule for extreme probability paper. *J. Geophys. Res.* **68**, 813–814 (1963).
53. Song, X.-P. et al. Global land change from 1982 to 2016. *Nature* **560**, 639–643 (2018).
54. Yang, W. et al. MODIS leaf area index products: from validation to algorithm improvement. *IEEE Trans. Geosci. Remote Sens.* **44**, 1885–1898 (2006).
55. Jung, M. et al. The FLUXCOM ensemble of global land-atmosphere energy fluxes. *Sci. Data* **6**, 74 (2019).
56. Li, X. & Xiao, J. A global, 0.05-degree product of solar-induced chlorophyll fluorescence derived from OCO-2, MODIS, and reanalysis data. *Remote Sens.* **11**, 517 (2019).
57. Hunter, J. D. Matplotlib: A 2d graphics environment. *Comput. Sci. Eng.* **9**, 90–95 (2007).

Acknowledgements

SO acknowledges the Basic Science Research Program through the National Research Foundation of Korea (NRF) funded by the Ministry of Education (RS-2023-00248706). Additional supports are given to SKP through the NRF Grant funded by the Korea government (MSIT) (NRF-2021R1A2C1095535) and by the Basic Science Research Program through the NRF funded by the Ministry of Education (2018R1A6A1A08025520) and by the Specialized university program for confluence analysis of Weather and Climate Data of the Korea Meteorological Institute (KMI) funded by the Korean government (KMA).

Author contributions

SO designed the study, performed the experiments, and drafted the manuscript. SKP discussed the results and contributed to the writing.

Competing interests

The authors declare no competing interests.

Additional information

Supplementary information The online version contains supplementary material available at https://doi.org/10.1038/s43247-024-01247-4.

Correspondence and requests for materials should be addressed to Seon Ki Park.

Peer review information *Communications Earth & Environment* thanks Shuo Wang and the other, anonymous, reviewer(s) for their contribution to the peer review of this work. Primary Handling Editors: Rodolfo Nóbrega and Aliénor Lavergne. A peer review file is available.